AN INTEGRATED APPROACH FOR SIMULATION AND PREDICTION OF LAND USE AND LAND COVER CHANGES AND URBAN GROWTH (CASE STUDY: SANANDAJ CITY IN IRAN)

Morteza Shabani[1], Shadman Darvishi[2], Hamidreza Rabiei-Dastjerdi[3,4]*, Seyed Ali Alavi[5], Tanupriya Choudhury[6], Karim Solaimani[1]

[1]Sari Agricultural Sciences and Natural Resources University, Institute of Remote Sensing and GIS, Sari, Iran; e-mails: Shabani@sanru.ac.ir; k.solaimani@sanru.ac.ir
[2]Aban Haraz Institute of Higher Education, Department of Remote Sensing and GIS, Amol, Iran; e-mail: sh_darvishi@yahoo.com
[3]University College Dublin (UCD), School of Architecture, Planning and Environmental Policy & CeADAR (Ireland's National Centre for Applied Data Analytics & AI), Belfield, Dublin, Ireland; e-mail: hamid.rabiei@ucd.ie
[4]Isfahan University of Medical Sciences, Social Determinants of Health Research Center, Isfahan, Iran
[5]Tarbiat Modares University, Department of Geography and Urban Planning, School of Humanity, Tehran, Iran; e-mail: a.alavi@modares.ac.ir
[6]University of Petroleum and Energy Studies (UPES), Department of Informatics, School of Computer Science, Dehradun, India; e-mail: tanupriya@ddn.upes.ac.in

Abstract: One of the growing areas in the west of Iran is Sanandaj city, the center of Kordestan province, which requires the investigation of the city's growth and the estimation of land degradation. Today, the combination of remote sensing data and spatial models is a useful tool for monitoring and modeling land use and land cover (LULC) changes. In this study, LULC changes and the impact of Sanandaj city growth on land degradation in geographical directions during the period 1989 to 2019 were investigated. Also, the accuracy of three models, artificial neural network-cellular automata (ANN-CA), logistic regression-cellular automata (LR-CA), and the weight of evidence-cellular automata (WOE-CA) for modeling LULC changes was evaluated, and the results of these models were compared with the CA-Markov model. According to the results of the study, ANN-CA, LR-CA, and WOE-CA models, with an accuracy of more than 80%, are efficient and effective for modeling LULC changes and growth of urban areas.

Keywords: land use and land cover change; artificial neural network; logistic regression; cellular automata; Sanandaj

1. Introduction

The continuous and ongoing process of urbanization has led to the fact that today more than half of the world's population lives in urban areas. By 2050, about 68% of the world's population will live in urban areas (United Nations, 2018). Since there is a strong relationship between urban population

---

*Corresponding author, e-mail: hamid.rabiei@ucd.ie

growth and agricultural land development, therefore, as the urban population increases, the need for food increases to the same extent. In order to fulfill urban dwellers' food security, many areas with natural coverage are converted to agricultural lands (Boudet et al., 2020; Valjarević et al., 2021; Zeaiean et al., 2005). The increase in the number of cities, the growth of urban areas, as well as the activities of urban dwellers have caused changes in land use and land cover (LULC) and natural environments in general (Mitsova et al., 2011; Sapena & Ruiz, 2019). LULC changes are one of the influential factors in the destruction of the environment and natural resources (Mucova et al., 2018). Among these effects are air quality reduction (Tao et al., 2018), soil erosion (Ouyang et al., 2018), changes in the hydrological cycle and water resources (Wang et al., 2020), increased runoff and flood (Lee & Brody, 2018), changes in land surface temperature, formation, and intensification of thermal islands in cities (Grigoraș & Urițescu, 2019). Also, there is an impact on the quality and level of groundwater (Khan et al., 2017), evapotranspiration (Odongo et al., 2019), climate changes, biodiversity (Verstegen et al., 2019), and human health (Xu et al., 2008). In Iran, a developing country, the number of cities from 496 urban points in 1986 reached 1,245 urban points in 2016 (Statistical Center of Iran, 2016). Also, the growth rate of urbanization was 54.3% in 1986 and 75% in 2018, which, according to the UN estimation, will reach 80% and 86% in 2030 and 2050, respectively (United Nations, Department of Economic and Social Affairs, Population Division, 2019). The unplanned growth of urban areas in Iran, as well as the lack of attention to LULC changes in recent years, have become a crucial environmental problem (Kourosh Niya et al., 2020). This problem is observed in many urban areas in Iran, especially in medium-sized growing cities. Sanandaj, the capital city of the Kordestan province, in the west of Iran, is one of these cities. From 1986 to 2016, two factors of population growth and migration (about 158,853 people) caused the spatial growth of the city. These factors have appeared due to the welfare amenities and economic facilities of Sanandaj compared to the surrounding cities and the political-administrative center of the Kordestan province (Statistical Center of Iran, 2016). In this area, one of the most important reasons for environmental degradation has been population growth and meeting its needs (Karimi & Boussauw, 2018) for optimal management and planning; it is necessary to study the trend of LULC change and growth of Sanandaj. Today, one of the accurate and efficient methods for understanding the trend of land cover changes is using remote sensing data (Gross et al., 2013). The use of satellite images, as well as the combination of these data with the Geographic Information System (GIS), is an effective tool to measure LULC changes in the past, present, and future of LULC changes (Alimohammadi et al., 2004; Amini et al., 2022; Rabiei-Dastjerdi et al., 2022). Since research on urban growth and LULC changes has led to the emergence of new spatial models in this field, it is necessary to investigate and evaluate these models. Therefore, the main questions of this research are:

- What has been the trend of LULC changes in Sanandaj during the 30 years (1989–2019)?
- In what geographical direction has the most land degradation caused by the growth of Sanandaj occurred?
- What will be the LULC changes and land degradation caused by the growth of Sanandaj until 2034?

To answer the research questions, the impact of Sanandaj growth on LULC degradation in the period of 30 years (1989–2019) was studied by Landsat images and GIS. Then, using artificial neural network-cellular automata (ANN-CA), logistic regression-cellular automata (LR-CA), and weight of evidence-cellular automata (WOE-CA) models, the trend of LULC change and growth of Sanandaj until 2034 was modeled, and the results of these models were compared with the CA-Markov model.

2. Material and methods

2.1. Study area

Sanandaj is located between 46˚59'45" east longitude and 35˚19'00" north latitude in the mountainous region of Zagros in western Iran. The altitude of this city is between 1,450 to 1,538 m a.s.l. and its area is 3,061.54 km^2 (Figure 1). This area has a semi-arid Mediterranean climate with an average annual rainfall of 500 mm (Iran Meteorological Organization, 2019). The city has had significant growth in recent years. According to census data, this growth, in addition to natural growth, has been due to the migration of villagers and the dwellers of small towns to the city. The population of Sanandaj city was 240,000, 318,000, and 414,000 people in 1989, 2004, and 2016, respectively (Statistical Center of Iran, 2016). In this study, environmental degradation, failure to pay attention to LULC changes, and high urbanization rates were the reasons for choosing this city as a case study.
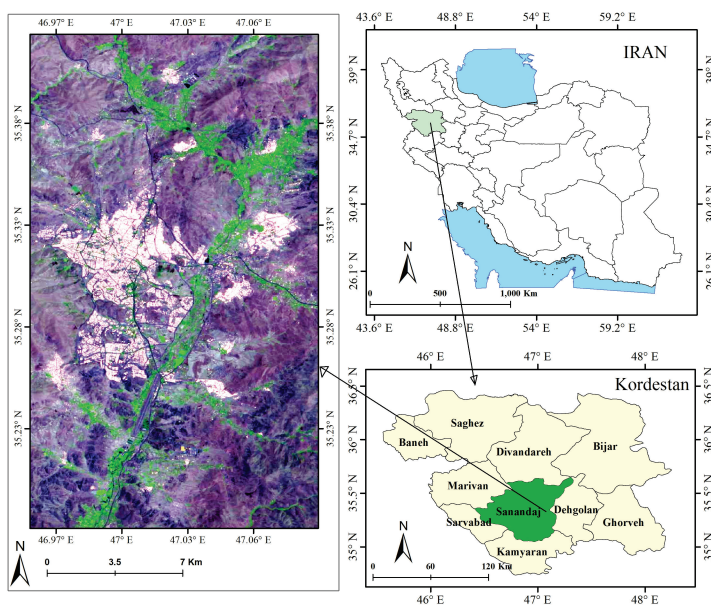

Figure 1. The geographical location of Sanandaj in Iran and Kordestan province.

2.2. Dataset

In this study, we used Landsat multispectral images (with minimum cloud cover and maximum vegetation density) to monitor and model LULC changes and the growth of Sanandaj (U.S. Geological Survey, 2019). The dates of images were selected from late May to early June (05/30/1989, 05/31/2004, and 06/02/2019) in two scenes (path/row: 167.35 and 167.36). Also, LULC vector maps, a topographic map with a scale of 1:250,000 and 16 features (Digital elevation model [DEM], Slope, Aspect, Distance from main road, Distance from main river, Distance from minor river, Distance from forest, Distance from agriculture, Distance from surface waters (lake, dam, and etc.), Distance from cemetery, Soil, Distance from green space (parks, grass, and etc.), Distance from major urban area, Distance from suburban area, Distance from residential area, and Distance from industrial and commercial centers, related to LULC changes and the growth of Sanandaj were used.
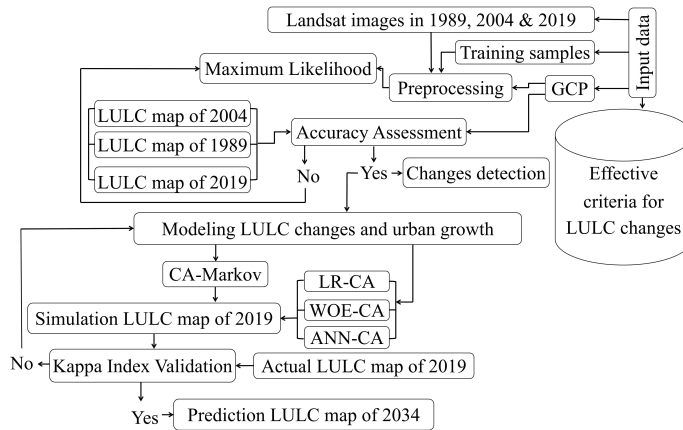
Figure 2. Flowchart of the research method.

2.3. Preprocessing images

The preprocessing of satellite images includes three steps. In the first step, the image mosaic operation was performed in ENVI software (Version 5.0.3; Exelis Visual Information Solutions, 2019). Then, the error of scan line corrector of the 2004 image was corrected using Landsat Gap fill extension (Hao et al., 2020). In the second step, geometric corrections of the images were performed. For this purpose, the 2019 image, first, was referenced using ground control points (collected from the topographic map with the scale of 1:250,000 and Global Positioning System (GPS) with the Root Mean Square Error (RMSE) of less than 0.3 pixels (Pal & Ziaul, 2017). Then the images of 1989 and 2004 were also referenced with the image of 2019 with the RMSE of less than 0.5 pixels (Shooshtari & Gholamalifard, 2015). In the third step, radiometric and atmospheric corrections of the images were performed. For this purpose, first, the digital numbers of the images were converted to Radiance, and then the Fast Line-of-sight Atmospheric Analysis of Hypercubes algorithm was applied to the images (Roy & Inamdar, 2019). This algorithm has been recommended to retrieve the reflected numbers from the radiance of multispectral images (Dube et al., 2014).

2.4. Classification images

After preprocessing images in order to prepare the LULC maps, the training samples with observing the overlap using field studies were collected from May 25 to June 15, 2019 with the help of GPS, interviews with local people, Google Earth images, and LULC vector maps. The images were then classified into five classes by applying the Maximum Likelihood algorithm in ENVI Software.

2.5. Preparation of spatial variations

The processing of spatial variables included the determination of coordinates, layers accuracy, distance determination, and normalization, which was done by ArcGIS software (Version 10.2; ESRI, 2019). LULC classes include water bodies (lake, river, dam reservoirs, and wetlands), built-up (urban, rural, industrial), vegetation (rangelands, forests, and green cover), agriculture (cropland, orchards, and irrigated agricultural lands), and bare areas.

2.6. Modeling LULC

The process of simulating LULC changes was done using the matrix of changes and maps of the potential of changes in 1989 and 2004 and the process of modeling changes was performed by using the matrix of changes and maps of the potential of changes in 2004 and 2019 and spatial variables. The matrix of changes and maps of the probability of changes were prepared using WOE, ANN, and LR models, and then by combining the results of these models with the CA model, spatial changes were simulated and modeled. Then the simulated map was validated using actual LULC map and ground control points in 2019 (Aneesha Satya et al., 2020).

2.7. Logistic regression

The logistic regression model provides an analysis of the relationships between multiple input variables and presents the relationships of independent and dependent variables as a number or set of numbers (Lakes et al., 2009). In this model, the dependent variable is binary (0 and 1). The value of 1 indicates the occurrence of an event, and a value of zero indicates the non-occurrence of an event (Lin et al., 2011).

$$f(z) = 1/1 + e^{-z} \tag{1}$$

$$P\{Y = 1|X\} = 1/1 + e^{-(\alpha + \sum_{i=1}^{k} \beta_i X_i)} \tag{2}$$

$$\beta = \beta_0 + \beta_1 + \beta_2 + \beta_3 + ... + \beta_n \tag{3}$$

$$X = X_0 + X_1 + X_2 + X_3 + ... + X_n \tag{4}$$

where $P\{Y = 1|X\}$ is the probability of the dependent variable (Y) being 1 (LULC change and urban growth), β and X are regression coefficients and independent variables (such as DEM, slope, distance to road, distance to river, etc.), respectively (Siddiqui et al., 2018).

2.8. Weights of evidence

The WOE model is a static method for calculating the weight of factors based on a linear logic of Bayes' theorem (Equation 5) used in environmental sciences, geology and natural disaster management, urban growth modeling, and LULC (Kourosh Niya et al., 2020). For the studies of LULC changes, this method calculates the weight of each factor affecting LULC changes based on the presence or absence of LULC changes in the area, which is mathematically shown as Equations 6 and 7 (Bonham-Carter, 1994).

$$P(f|c) = p(c|f) \times p(c) / p(f) \tag{5}$$

where p(f) if the probability of occurrence of event f, p(c) is the probability of occurrence of event c, P(f|c) is the probability of occurrence of event f when event c has occurred and P(f|c) is also the probability of occurrence of event c when event f has occurred.

$$W_i^+ = \ln[P(F|C) \, / \, (F|\overline{C})] \tag{6}$$

$$W_i^- = \ln[P(\overline{F}|C) \, / \, (\overline{F}|\overline{C})] \tag{7}$$

where P indicates the probability, F is the presence of a factor predicting LULC change, $\overline{F}$ is the absence of a factor predicting LULC changes. C and $\overline{C}$ also indicate the presence and absence of LULC changes in the area, respectively. In this model, the positive weight W_i^+ indicates the effectiveness of factors in LULC changes and W_i^- indicates the ineffectiveness of factors in LULC changes. The difference between positive and negative weights is the contrast (C) of weight (Equation 8), which shows the relationship between factors and LULC changes (Regmi et al., 2014).

$$C = W^+ - W^- \tag{8}$$

2.9. Markov chain (MC)

This model calculates the trend of changes of variables (agriculture, urban, vegetation, etc.) in two periods as a random process and models the trend of future changes using past changes. Considering that LULC changes occur in a temporal and spatial period, this model has many applications to specify the trend of these changes, but regarding that the matrix results of this model do not show spatial changes, the results of this model are combined with that of the cellular automata model (Yang et al., 2012). Mathematically, the MC model is described according to Equations 9 and 10.

$$E_{t+1} = P_{ij} \times E_t \tag{9}$$

$$P = (P_{ij}) = \begin{Bmatrix} P_{11} & P_{12} & P_{1m} \\ P_{21} & P_{22} & P_{2m} \\ P_{m1} & P_{n2} & P_{mm} \end{Bmatrix}$$

$$\sum_{i=1}^{m} P_{ij} = 1, \quad j = 1, ..., m \tag{10}$$

where, E_t is the LULC state at the time of t, E_{t+1} is the LULC state at the time of $t + 1$, P_{ij} is the matrix of conversion probability from LULC i to LULC j, and m is the number of classes in the LULC map. P_{ij} values are between 0 and 1 and are as $1 \leq P_{ij} \leq 0$ (Mohamed & Worku, 2020).

2.10. Artificial neural network (ANN)

An ANN is a model for information processing. This system is made up of a large number of neurons that act coordinately to solve a problem. Each one of the neurons receives input information and, after processing, produces an output. An ANN usually consists of three layers, including the input layer, the middle layer, and the output layer. Normally, the neurons in each layer are connected to all the neurons in the adjacent layer through a directional connection, and information is transmitted

between them through these connections. Each of these connections has the weight assigned to its own, which is multiplied by the information transmitted from one neuron to another. Each neuron receives weighted outputs from the neurons in the previous layer, all of which generate neuron input (Pourghasemi & Gokceoglu, 2019).

$$\text{net}_j(k,t) = \sum_i w_{ij,\,k}\, x_i'(k,t) \tag{11}$$

$$P(k,t,l) = \sum_j w_{j,l} 1 \,/\, 1 + e^{-netj(k,t)} \tag{12}$$

where w_{ij} is the weight of the connection between the neurons i and j, $x_i'(k,t)$ is a descriptive scale to the neuron i, k is the cell, t is the time of t, $P(k,t,l)$ is the probability of converting a use in a LULC map for cell k at the time of t, and $w_{j,l}$ is the weight between the hidden layer and the output layer (Saputra & Lee, 2019).

2.11. Cellular automata (CA)

This model shows the spatial distribution of LULC changes and the growth of urban areas well, and the output MC, ANN, LR, WOE, and SM models which are used as model input (Mohamed & Worku, 2020). This model has five main components (Equation 13): cellular network, cell status, neighborhood, time, and transfer rules (White & Engelen, 2000).

$$\{E_{t+1}\} = L\{(E_t) \times (N_t^h) \times (S)\} \tag{13}$$

where E_{t+1} and E_t, are the cell state at the time of t + 1, t, N and S, respectively, refer to the neighborhood and the competency of a cell for LULC changes and urban growth, and L, t, and h, are the rules of transfer, the temporal stages of the cell in temporal space, and the size of the neighborhood (Siddiqui et al., 2018).

2.12. Accuracy assessment of LULC maps

In this study, GPS data were used to assess the accuracy of LULC maps. The parameters of overall accuracy, producer accuracy, user accuracy, and Kappa coefficient of LULC were calculated (Belay & Mengistu, 2019; Das et al., 2021).

2.13. Validation and comparison of models

Before implementing the LULC changes prediction process and providing accurate and reliable results, first, the LULC map in 2019 was simulated using CA-Markov, ANN-CA, LR-CA, and WOE-CA models. After that, the simulated maps, using the real LULC map in 2019 and ground truth data (collected using GPS), were validated by IDRISI Terrset and QGIS2.18-MOLUSCE Plugin software (QGIS Development Team, 2016; Figure 2). The accuracy rate of the simulated maps was calculated in the form of Kappa coefficients (k no, k location, k location strata, k standard, overall kappa). In addition to calculating kappa coefficients, the percentage of accuracy between the two simulated maps and the real LULC map was also examined. After simulating the LULC map in 2019 using ANN-

CA, LR-CA, WOE-CA, and CA-Markov models and validating the models with the LULC map in 2019, the results of the models were compared with the CA-Markov model.

3. Results and discussion

3.1. Accuracy assessment results

Before monitoring LULC changes and urban growth, it is necessary to examine the results of the overall accuracy of LULC maps (Figure 3). Table 1 shows the overall accuracy and kappa coefficients, and it shows acceptable accuracy of LULC maps because the minimum acceptable overall accuracy in LULC maps is 85%, and the excellent agreement of kappa coefficients is ≥ 75% (Hishe et al., 2020).
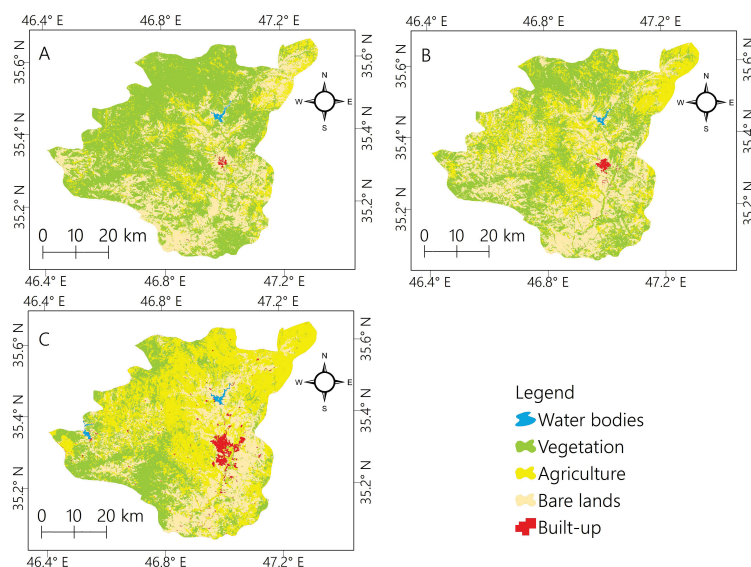

Figure 3. LULC maps in 1989 (A), 2004 (B), and 2019 (C).

Table 1. Results of accuracy assessment and kappa coefficient (%)

Years/Overall accuracy		User accuracy					Producer accuracy					Kappa coefficient
		1	2	3	4	5	1	2	3	4	5	
1989	90	86	83	94	93	92	80	100	100	81	92	87
2004	92	100	100	81	100	83	85	100	100	82	83	90
2019	87	86	83	94	87	86	80	83	100	81	92	84

Note. 1 = Water bodies, 2 = Built-up, 3 = Vegetation, 4 = Agriculture, 5 = Bare lands.

3.2. Change detection

In the 30-year period (1989–2019), LULC area showed that vegetation decreased by 31.17% and agriculture increased by 32.34 %. The highest decrease in vegetation lands was in the period 1989 to 2004 (16.36%), and the highest increase in agricultural lands was in the period 2004 to 2019 (20.32%). Bare lands increased in the period 1989 to 2004 but decreased in the period 2004 to 2019, which was the opposite trend in the water areas. Residential land has increased in the period of 30 years (Table 2).

Table 2. LULC changes and area in the period from 1989 to 2019 (ha)

Period/LULC	Water bodies	Built-up	Vegetation	Agriculture	Bare lands
1989	672.97	496.42	175,758	40,308	88,919.5
2004	547.64	1,224.55	125,655	77,112.7	101,615
2019	1,155.02	5,946.17	80,316.4	139,328	79,409.3
Changes LULC (1989 to 2004)	−125.33	728.13	−50,103	36,804.7	12,695.5
Changes LULC (2004 to 2019)	607.38	4,721.62	−45,338.6	62,215.3	−22,205.7
Changes LULC (1989 to 2019)	482.05	5,449.75	−95,441.6	99,020	−9,510.2

In this area, the growth of agricultural lands (62,215.3 ha) in the period 2004 to 2019 was consistent with the population growth of Sanandaj (84,225 people) in the period 2006 to 2016. This shows that citizens need food and food security.

The trend of land conversion in Sanandaj with 0.88% and 0.84% accuracy shows that in the 30-year period, 59,728.95 ha of vegetated lands and 28,922.58 ha of barren lands have been converted into agricultural lands. Most of these conversions were in the period 2004 to 2019 and in accordance with the increase in the population of Sanandaj. In the 30-year period, the conversion rate of vegetated lands and barren lands reduced their area. This decrease was slighter in barren lands but more in vegetation lands. In this period, 16,552.26 ha of agricultural lands were converted to vegetation and 3,945.33 ha to barren lands. In addition to the conversion of vegetation lands to agriculture, the conversion of vegetation lands to barren was another important factor in reducing vegetation lands in the region. In the period of 30 years, 48,136.68 ha of vegetation lands became barren lands, and 28,007.64 ha of barren lands became vegetation (Table 3).

Table 3. LULC conversions rate (ha)

Period	LULC	Conversions	LULC	Conversions
1989 to 2004	Water bodies to build-up	0.09	Vegetation to agriculture	34,490.70
	Water bodies to vegetation	12.33	Vegetation to bare lands	35,454.87
	Water bodies to agriculture	1.08	Agriculture to water bodies	-
	Water bodies to bare lands	125.73	Agriculture to vegetation	8,906.22
	Built-up to water bodies	-	Agriculture to bare lands	1,425.69
	Built-up to vegetation	9.36	Bare lands to water bodies	11.07
	Built-up to agriculture	0.09	Bare lands to vegetation	11,104.47
	Built-up to bare lands	0.03	Bare lands to agriculture	12,568.68
	Vegetation to water bodies	0.99	-	-
2004 to 2019	Water bodies to build-up	1.53	Vegetation to agriculture	56,279.25
	Water bodies to vegetation	-	Vegetation to bare lands	12,681.81
	Water bodies to agriculture	0.18	Agriculture to water bodies	163.89
	Water bodies to bare lands	1.26	Agriculture to vegetation	7,646.04
	Built-up to water bodies	-	Agriculture to bare lands	2,519.64
	Built-up to vegetation	6.21	Bare lands to water bodies	308.07
	Built-up to agriculture	14.94	Bare lands to vegetation	16,903.17
	Built-up to bare lands	80.55	Bare lands to agriculture	16,353.90
	Vegetation to water bodies	144.90	-	-

3.3. Impact of urban growth on LULC degradation

In the present study, the growth of Sanandaj was examined based on the center of this city, and the amount of land destruction caused by the growth of Sanandaj during the period from

1989 to 2019 was investigated. For this purpose, the growth map was drawn using GIS and field studies and a detailed plan in various geographical directions. The results showed that the growth of Sanandaj with the highest rate of LULC destruction from 1989 to 2004, and the focus was more on the northwest, west, and south directions. From 2004 to 2019, the focus was more on the south, southeast, east, and southwest directions (Figure 4).
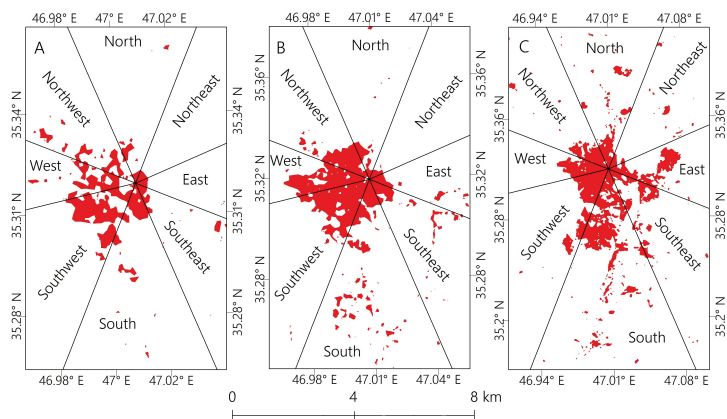

Figure 4. Map of Sanandaj area in 1989 (A), 2004 (B), and 2019 (C).

To investigate the location of land degradation due to the growth of Sanandaj, the map of the Sanandaj area in 2004 and 2019 overlapped with LULC maps in 1989 and 2004 (Figure 5). Investigating city growth maps shows that the growth of this city from 2004 to 2019, in addition to the destruction of barren areas, vegetation lands, and agricultural lands around the city, was higher from 1989 to 2004. Also, the highest destruction rate of vegetation lands has been in urban areas in the south, southeast, east, and north directions. The highest percentage of destruction of agricultural lands to urban areas has been in the north, south, and southwest directions. On the other hand, the highest barren land destruction in urban areas has occurred in the southern direction (Figure 5).
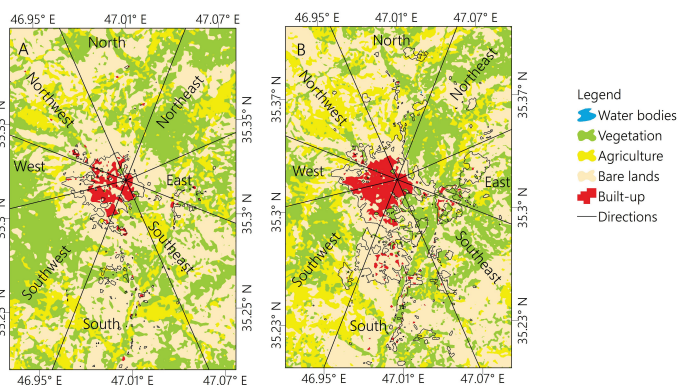

Figure 5. LULC map of Sanandaj in 1989 (A) and 2004 (B) and the growth of this city in 2004 (A) and 2019 (B) in geographical directions.

3.4. Modeling LULC change and urban growth

To assess the accuracy of the models, the 2019 simulated maps were validated with WOE-CA, ANN-CA, LR-CA, and CA-Markov models using the 2019 real LULC map and ground truth data (collected using GPS). According to the extracted results, the total kappa coefficients of WOE-CA, ANN-CA, LR-CA, and CA-Markov models obtained are 0.88%, 0.86%, 0.80%, and 0.88%, respectively.

Also, the accuracy rate of WOE-CA, ANN-CA, LR-CA, and CA-Markov models compared to the real LULC map has been 92.11%, 91.04%, 82.15%, and 90.41%, respectively. Based on these results, the accuracy of WOE-CA, ANN-CA, LR-CA, and CA-Markov models for predicting LULC changes is acceptable. Also, the investigation of the accuracy of the mentioned models with the CA-Markov model (with an accuracy of 90.41%) shows that the accuracy of the WOE-CA and ANN-CA models was close to CA-Markov model, but the accuracy of the LR-CA model compared to WOE-CA and ANN-CA models was lower (Table 4). After calculating the validation results of the models, the LULC map and the growth of Sanandaj for 2034 were predicted (Figure 6).

Table 4. Report of Kappa coefficients of the models used

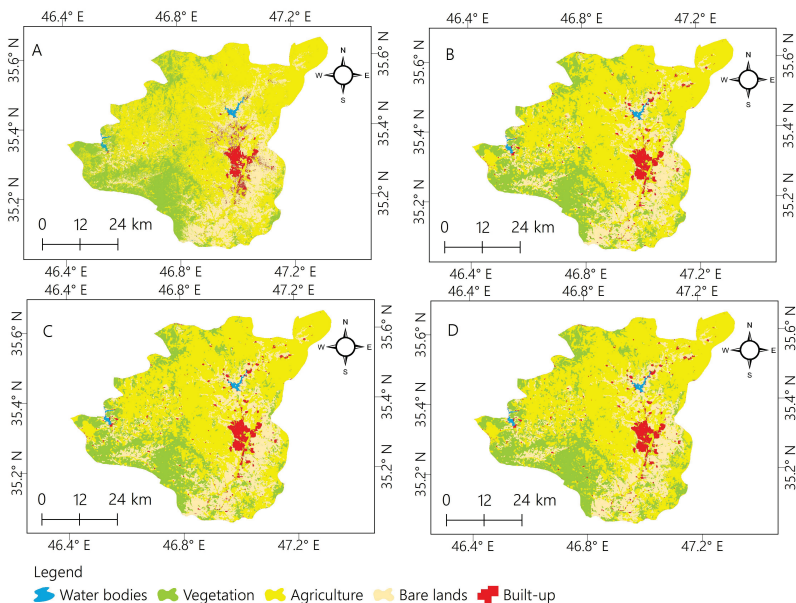| Methods	k no	k location	k strata location	k standard	overall kappa	% of correctness
CA-Markov	.88	.90	.90	.86	.86	90.41
CA-LR	.87	.85	.85	.84	.80	82.15
CA-WOE	.90	.96	.96	.88	.88	92.11
CA-ANN	.88	.93	.93	.85	.86	91.04

Figure 6. Predicted LULC map for 2034 based on LR-CA (A),
CA-Markov (B), ANN-CA (C), and WOE-CA (D) models.

For this purpose, the matrix of conversion probability of uses was formed for the two periods; from 1989 to 2004 and from 2004 to 2019. According to the matrix, the probability of conversion of uses in the period from 1989 to 2004, the highest rate of conversion of one use to another use is related to agricultural lands and vegetation, that 0.2195% of agriculture was converted to vegetation. On the other hand, 0.1966% of vegetation lands was converted to agricultural lands. The conversion of vegetation lands and water areas to barren areas in this period was 0.2020% and 0.1872%, respectively, the point that refers to the loss of vegetation and the reduction of the water of rivers and other water resources and the conversion of these areas to barren lands. In the period from 2004 to 2019, the highest rate of use conversion, like the previous period, is also related to vegetation and agricultural lands, and in this period, 0.4483% of vegetation lands was converted to agricultural lands, which is the highest amount among all uses. Also, 0.1664% and 0.1610%, respectively, of barren lands were converted to vegetation lands and agricultural lands in this period. Land area in the predicted maps for 2034 shows that vegetation lands and barren areas will have a decreasing trend, and agricultural lands, urban areas, and water areas will have an increasing trend by 2034 (Table 5).

Table 5. Predicted area of LULC classes in 2034 (ha)

Models/LULC types	Water bodies	Built-up	Vegetation	Agriculture	Bare lands
CA-LR	795.24	8,478.85	59,423.3	168,621.3	68,836.2
CA-Markov	1,159.69	8,944.03	63,215.1	169,320.27	63,515.8
CA-ANN	1,158.84	8,932.71	63,194.8	169,470.74	63,397.8
CA-WOE	1,158.84	8,971.86	68,279.6	169,343.19	58,401.4

The decreasing trend of vegetation lands based on WOE-CA, ANN-CA, and CA-Markov models compared to 2019 will be 3.93% and 5.59%, and also the increasing trend of agricultural lands will be 9.81%, 9.86%, and 9.80%, respectively. Barren lands, like vegetation lands, will also have a decreasing trend compared to 2019.

The area of vegetation and barren lands in the LR-CA model, like the WOE-CA, ANN-CA, and CA-Markov models, also shows a decreasing trend for 2034, and these lands have decreased by 6.83% and 3.45%, respectively, compared to 2019. Also, the area of agricultural lands and urban areas will increase by 9.57% and 0.79% by 2034, respectively. Based on the validation results (Section 3.4.), the predicted LULC area in WOE-CA, ANN-CA, and CA-Markov models is more accurate than the LR-CA model due to the accuracy of these models. Also, land conversions kappa coefficients in the period from 2019 to 2034 show that the accuracy of WOE-CA, ANN-CA, CA-Markov, and LR-CA models are 0.89%, 0.89%, 0.88%, and 0.72%, respectively, which, like the validation results, indicate the high accuracy of CA-WOE, CA-ANN, and CA-Markov models. Following this issue is the LULC predicted conversions trend for the period from 2019 to 2034 based on the WOE-CA, ANN-CA, and CA-Markov models.

According to the CA-Markov model, 22,475.52 ha and 8,025.39 ha of vegetation and barren lands will be converted to agricultural lands, which will be the highest conversion rate at the area level. This trend will also be present in the ANN-CA model, and based on this model, 22,489.56 ha and 8,733.15 ha will be converted from vegetation lands and barren areas to agricultural lands, respectively. In the WOE-CA model, in addition to the point that the trend of conversion of vegetation lands and barren areas to agricultural lands shows a significant amount, the conversion of barren lands to vegetation will also be 10,225.71 ha according to this model. According to the CA-Markov, ANN-CA, and WOE-CA models, 113.49

ha, 333.27 ha, and 446.13 ha, respectively, of agricultural lands will be converted to vegetation, and 466.20 ha, 36.09 ha, 411.21 ha of agricultural lands will be converted to barren lands. In general, the growth of agricultural lands, which has caused the destruction of vegetation and barren lands, has been mostly due to the spatial and population growth of Sanandaj to respond to the food security of urban residents. According to the results, the spatial growth of Sanandaj and agricultural lands during the study period (1989 to 2034) has been consistent.

3.5. Projected impact of urban growth on LULC degradation

The investigation of the growth trend of Sanandaj in the period from 2019 to 2034, as in the previous period, will indicate the continuous growth of this city, especially in the southern direction. Based on the results of WOE-CA, ANN-CA, and CA-Markov models, the Sanandaj area will grow 0.96%, 0.94%, and 0.95%, respectively, compared to 2019. The continuous growth of Sanandaj until 2034, as in previous periods, will cause land degradation, and in this period (2019 to 2034), compared to previous periods, the destruction of barren lands and agricultural lands will be more than vegetation lands. The unplanned growth of Sanandaj will continue in the southern direction as in previous periods, and this will cause more land degradation in this direction than in other directions (Figure 7). According to WOE-CA, ANN-CA, and CA-Markov models, 22.90%, 25.58%, and 41.52% of the total conversion of agricultural lands, respectively, 24.87%, 24.57%, and 24.28% of the total conversion of barren lands to urban areas will be in this direction.
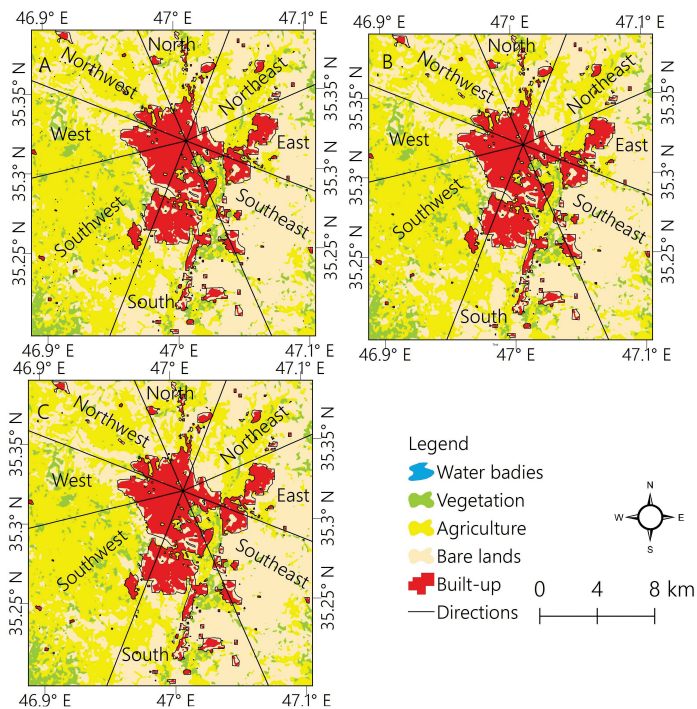

Figure 7. Map of the growing trend of Sanandaj in the period from 2019 to 2034 based on CA-WOE (A), CA-ANN (B), and CA-Markov (C) models.

4. Conclusion

In the present study, the accuracy of ANN-CA, WOE-CA, and LR-CA models for simulation and modeling of LULC changes and the growth of Sanandaj city in Kordestan province of Iran was investigated and then the results of these models were compared with CA-Markov model. After extracting LULC maps in 1989, 2004, and 2019, the results of investigating the maps with an accuracy of more than 85% indicated the decreasing trend of vegetation and barren lands and the increasing trend of agricultural, residential lands, and water areas during a 30-year period. Also, the investigation of land destruction due to the growth of Sanandaj showed that the unplanned growth of the city has caused the destruction of vegetation lands, agricultural lands, and barren areas and considering the further growth of Sanandaj in the southern directions, land destruction in these directions has been more than in other directions. The accuracy of the models also showed that the WOE-CA, ANN-CA, and LR-CA models (92.11%, 91.04%, and 82.15%, respectively) have high accuracy for modeling LULC change and the growth of urban areas, which is in accordance with the results of Grigoras and Uritescu (2019) and Mucova et al. (2018); but the LR-CA model had a relatively lower accuracy compared to other models. The results of comparing the accuracy of the WOE-CA, ANN-CA, and LR-CA models with the CA-Markov model showed that the accuracy of the WOE-CA and ANN-CA models were closer to the CA-Markov model. According to the results of the models, vegetation lands will have a decreasing trend, and agricultural lands and urban areas will also have an increasing trend until 2034. The downward trend of agricultural land conversion in many regions of Iran was reported in the studies of Kourosh Niya et al. (2020) and Shooshtari and Gholamalifard (2020). As the growth trend of Sanandaj until 2034 shows, if the growth of this city is unplanned, like in previous periods, the destruction of lands due to the growth of the city will also continue until 2034, and many agricultural lands and barren areas will be destroyed, especially in the southern directions. In general, the results of LULC maps and models show that the LULC status and the growth of Sanandaj require necessary attention and careful planning to manage these changes, and in case of the lack of accurate planning for the LULC changes of this area, the destruction of vegetation lands will continue as in the previous periods, and vegetation lands will be destroyed in the near future. Destruction of vegetation lands can create the basis for the emergence of many environmental and natural problems. Considering that the conversion of vegetation lands to agricultural lands has been one of the effective factors in the destruction of vegetation lands at the area level, one of the effective programs in this field is the allocation of barren areas around Sanandaj to agricultural lands. This action will reduce the destruction of vegetation lands, provide food security for urban dwellers, and prevent the emergence of many environmental problems. Future relevant studies should be modeled based on the factor in the study area to compare the result of urban expansion and LULC dynamics. In addition, other driving factors such as population dynamics, land market demand, process supply patterns, and per capita income should be incorporated into the modeling procedure.

References

Alimohammadi, A., Rabiei, H. R., & Zeaiean Firouzabadi, P. (2004). A new approach for modeling uncertainty in remote sensing change detection process. In B. S. Anders (Ed.), *Proceedings of the 12th International Conference on Geomatics – Geospatial Information Research: Bridging the Pacific and Atlantic* (pp. 505–508). T. Academic. http://giscience.hig.se/binjiang/geoinformatics/files/p503.pdf

Amini, S., Saber, M., Rabiei-Dastjerdi, H., & Homayouni, S. (2022). Urban Land Use and Land Cover Change Analysis Using Random Forest Classification of Landsat Time Series. *Remote Sensing*, *14*(11), Article 2654. https://doi.org/10.3390/rs14112654

Aneesha Satya, B., Shashi, A., & Deva, P. (2020). Future land use land cover scenario simulation using open-source GIS for the city of Warangal, Telangana, India. *Applied Geomatics, 12*, 281–290. https://doi.org/10.1007/s12518-020-00298-4

Belay, T., & Mengistu, D. A. (2019). Land use and land cover dynamics and drivers in the Muga watershed, Upper Blue Nile basin, Ethiopia. *Remote Sensing Applications: Society and Environment, 15*, Article 100249. https://doi.org/10.1016/j.rsase.2019.100249

Bonham-Carter, G. F. (1994). *Geographic Information Systems for Geoscientists, Modelling with GIS*. Pergamon Press.

Boudet, F., MacDonald, G. K., Robinson, B. E., & Samberg, L. H. (2020). Rural-urban connectivity and agricultural land management across the Global South. *Global Environmental Change, 60*, Article 101982. https://doi.org/10.1016/j.gloenvcha.2019.101982

Das, N., Mondal, P., Sutradhar, S., & Ghosh, R. (2021). Assessment of variation of land use/land cover and its impact on land surface temperature of Asansol subdivision. *The Egyptian Journal of Remote Sensing and Space Science, 24*(1), 131–149. https://doi.org/10.1016/j.ejrs.2020.05.001

Dube, T., Gumindoga, W., & Chawira, M. (2014). Detection of land cover changes around Lake Mutirikwi, Zimbabwe, based on traditional remote sensing image classification techniques. *African Journal of Aquatic Science, 39*(1), 89–95. https://doi.org/10.2989/16085914.2013.870068

ESRI. (2019). *ArcGIS* (Version 10.2) [Computer software]. https://www.esri.com/en-us/arcgis/about-arcgis/overview

Exelis Visual Information Solutions. (2019). *ENVI* (Version 5.0.3) [Computer software]. https://envi.software.informer.com/download/#download_content

Grigoraş, G., & Uriţescu, B. (2019). Land Use/Land Cover changes dynamics and their effects on Surface Urban Heat Island in Bucharest, Romania. *International Journal of Applied Earth Observation and Geoinformation, 80*, 115–126. https://doi.org/10.1016/j.jag.2019.03.009

Gross, D., Dubois, G., Pekel, J.-F., Mayaux, P., Holmgren, M., Prins, H. H. T., Rondinini, C., & Boitani, L. (2013). Monitoring land cover changes in African protected areas in the 21st century. *Ecological Informatics, 14*, 31–37. https://doi.org/10.1016/j.ecoinf.2012.12.002

Hao, Y., Chen, Z., Huang, Q., Li, F., Wang, B., & Ma, L. (2020). Bidirectional Segmented Detection of Land Use Change Based on Object-Level Multivariate Time Series. *Remote Sensing, 12*(3), Article 478. https://doi.org/10.3390/rs12030478

Hishe, S., Bewket, W., Nyssen, J., & Lyimo, J. (2020). Analyzing past land use land cover change and CA-Markov based future modeling in the Middle Suluh Valley, Northern Ethiopia. *Geocarto International, 35*(3), 225–255. https://doi.org/10.1080/10106049.2018.1516241

Iran Meteorological Organization. (2019). *Climate of Sanandaj city*. Retrieved October 31, 2022, from https://www.irimo.ir

Karimi, N., & Boussauw, K. (2018). Sanandaj, Iran. *Cities, 72*(Part B), 261–273. https://doi.org/10.1016/j.cities.2017.09.004

Khan, A., Khan, H. H., & Umar, R. (2017). Impact of land-use on groundwater quality: GIS-based study from an alluvial aquifer in the western Ganges basin. *Applied Water Science, 7*, 4593–4603. https://doi.org/10.1007/s13201-017-0612-7

Kourosh Niya, A., Huang, J., Kazemzadeh-Zow, A., Karimi, H., Keshtkar, H., & Naimi, B. (2020). Comparison of three hybrid models to simulate land use changes: a case study in Qeshm Island, Iran. *Environmental Monitoring and Assessment, 192*, Article 302. https://doi.org/10.1007/s10661-020-08274-6

Lakes, T., Müller, D., & Krüger, C. (2009). Cropland change in southern Romania: a comparison of logistic regressions and artificial neural networks. *Landscape Ecology, 24*, Article 1195. https://doi.org/10.1007/s10980-009-9404-2

Lee, Y., & Brody, S. D. (2018). Examining the impact of land use on flood losses in Seoul, Korea. *Land Use Policy, 70*, 500–509. https://doi.org/10.1016/j.landusepol.2017.11.019

Lin, Y.-P., Chu, H.-J., Wu, Ch.-F., & Verburg, P. H. (2011). Predictive ability of logistic regression, auto-logistic regression and neural network models in empirical land-use change modeling – a case study. *International Journal of Geographical Information Science, 25*(1), 65–87. https://doi.org/10.1080/13658811003752332

Mitsova, D., Shuster, W., & Wang, X. (2011). A cellular automata model of land cover change to integrate urban growth with open space conservation. *Landscape and Urban Planning*, *99*(2), 141–153. https://doi.org/10.1016/j.landurbplan.2010.10.001

Mohamed, A., & Worku, H. (2020). Simulating urban land use and cover dynamics using cellular automata and Markov chain approach in Addis Ababa and the surrounding. *Urban Climate, 31*, Article 100545. https://doi.org/10.1016/j.uclim.2019.100545

Mucova, S. A. R., Filho, W. L., Azeiteiro, U. M., & Pereira, M. J. (2018). Assessment of land use and land cover changes from 1979 to 2017 and biodiversity & land management approach in Quirimbas National Park, Northern Mozambique, and Africa. *Global Ecology and Conservation, 16*, Article e00447. https://doi.org/10.1016/j.gecco.2018.e00447

Odongo, V. O., van Oel, P. R., van der Tol, C., & Su, Z. (2019). Impact of land use and land cover transitions and climate on evapotranspiration in the Lake Naivasha Basin, Kenya. *Science of the Total Environment, 682*, 19–30. https://doi.org/10.1016/j.scitotenv.2019.04.062

Ouyang, W., Wu, Y., Hao, Z., Zhang, Q., Bu, Q., & Gao, X. (2018). Combined impacts of land use and soil property changes on soil erosion in a mollisol area under long-term agricultural development. *Science of The Total Environment, 613–614*, 798–809. https://doi.org/10.1016/j.scitotenv.2017.09.173

Pal, S., & Ziaul, S. (2017). Detection of land use and land cover change and land surface temperature in English Bazar urban center. *The Egyptian Journal of Remote Sensing and Space Science, 20*(1), 125–145. https://doi.org/10.1016/j.ejrs.2016.11.003

Pourghasemi, H. R., & Gokceoglu, C. (2019). *Spatial Modeling in GIS and R for Earth and Environmental Sciences*. Elsevier press.

QGIS Development Team. (2016). *QGIS2.18-MOLUSCE Plugin software* [Computer software]. https://plugins.qgis.org/plugins/molusce/

Rabiei-Dastjerdi, H., Amini, S., McArdle, G., & Homayouni, S. (2022). City-region or city? That is the question: modelling sprawl in Isfahan using geospatial data and technology. *GeoJournal*, *87*, 1–21. https://doi.org/10.1007/s10708-021-10554-8

Regmi, A. D., Devkota, K. C., Yoshida, K., Pradhan, B., Pourghasemi, H. R., Kumamoto, T., & Akgun, A. (2014). Application of frequency ratio, statistical index, and weights-of-evidence models and their comparison in landslide susceptibility mapping in Central Nepal Himalaya. *Arabian Journal of Geosciences, 7*, 725–742. https://doi.org/10.1007/s12517-012-0807-z

Roy, A., & Inamdar, A. B. (2019). Multi-temporal Land Use Land Cover (LULC) change analysis of a dry semi-arid river basin in western India following a robust multi-sensor satellite image calibration strategy. *Heliyon, 5*(4), Article e01478. https://doi.org/10.1016/j.heliyon.2019.e01478

Sapena, M., & Ruiz, L. A. (2019). Analysis of land use/land cover spatio-temporal metrics and population dynamics for urban growth characterization. *Computers, Environment and Urban Systems, 73*, 27–39. https://doi.org/10.1016/j.compenvurbsys.2018.08.001

Saputra, M. H., & Lee, H. S. (2019). Prediction of Land Use and Land Cover Changes for North Sumatra, Indonesia, Using an Artificial Neural Network-Based Cellular Automaton. *Sustainability, 11*(11), Article 3024. https://doi.org/10.3390/su11113024

Shooshtari, S. J., & Gholamalifard, M. (2015). Scenario-based land cover change modeling and its implications for landscape pattern analysis in the Neka Watershed, Iran. *Remote Sensing Applications: Society and Environment, 1*, 1–19. https://doi.org/10.1016/j.rsase.2015.05.001

Siddiqui, A., Siddiqui, A., Maithani, S., Jha, A. K., Kumar, P., & Srivastav, S. K. (2018). Urban growth dynamics of an Indian metropolitan using CA Markov and Logistic Regression. *The Egyptian Journal of Remote Sensing and Space Sciences, 21*(3), 229–236. https://doi.org/10.1016/j.ejrs.2017.11.006

Statistical Center of Iran. (2016). *Census statistics*. https://www.amar.org.ir

Tao, H., Xing, J., Zhou, H., Chang, X., Li, G., Chen, L., & Li, J. (2018). Impacts of land use and land cover change on regional meteorology and air quality over the Beijing-Tianjin-Hebei region, China. *Atmospheric Environment, 189*, 9–21, https://doi.org/10.1016/j.atmosenv.2018.06.033

United Nations, Department of Economic and Social Affairs, Population Division. (2019). *World Urbanization Prospects: The 2018 Revision (ST/ESA/SER.A/420)*. United Nations.

U.S. Geological Survey. (2019). *Landsat images time series and Shuttle Radar Topography Mission Digital elevation datasets*. Retrieved from https://earthexplorer.usgs.gov

Valjarević, A., Filipović, D., Živković, D., Ristić, N., Božović, J., & Božović, R. (2021). Spatial Analysis of the Possible First Serbian Conurbation. *Applied Spatial Analysis and Policy*, *14*(1), 113–134. https://doi.org/10.1007/s12061-020-09348-1

Verstegen, J. A., van der Laan, C., Dekker, S. C., Faaij, A. P. C., & Santos, M. J. (2019). Recent and projected impacts of land use and land cover changes on carbon stocks and biodiversity in East Kalimantan, Indonesia. *Ecological Indicators, 103*, 563–575. https://doi.org/10.1016/j.ecolind.2019.04.053

Wang, X., Zhang, B., Xu, X., & He, C. (2020). Regional water-energy cycle response to land use/cover change in the agro-pastoral ecotone, Northwest China. *Journal of Hydrology, 580*, Article 124246. https://doi.org/10.1016/j.jhydrol.2019.124246

White, R., & Engelen, G. (2000). High-resolution integrated modelling of the spatial dynamics of urban and regional systems. *Computer, Environment and Urban Systems, 24*(5), 383–400. https://doi.org/10.1016/S0198-9715(00)00012-0

Xu, J., Sharma, R., Fang, J., & Xu, Y. (2008). Critical linkages between land-use transition and human health in the Himalayan region. *Environment International, 34*(2), 239–247. https://doi.org/10.1016/j.envint.2007.08.004

Yang, X., Zheng, X.-Q., & Lv, L.-N. (2012). A spatiotemporal model of land use change based on ant colony optimization, Markov chain and cellular automata. *Ecological Modelling, 233*, 11–19. https://doi.org/10.1016/j.ecolmodel.2012.03.011

Zeaiean, P., Rabiei, H. R., & Alimohamadi, A. (2005). Detection of Land Use/Cover Changes of Isfahan by Agricultural Lands Around Urban Area Using Remote Sensing and GIS Technologies. *The Journal of Spatial Planning*, *9*(4), 41–54. https://hsmsp.modares.ac.ir/article-21-6077-en.html